Technical Report

TR-98-17

Groundwater degassing in fractured rock:

Modelling and data comparison

Jerker Jarsjö and Georgia Destouni

Water Resources Engineering
Royal Institute of Technology, Stockholm

November 1998

Svensk Kärnbränslehantering AB
Swedish Nuclear Fuel
and Waste Management Co
Box 5864
SE-102 40 Stockholm Sweden
Tel 08-459 84 00
+46 8 459 84 00
Fax 08-661 57 19
+46 8 661 57 19

Groundwater degassing in fractured rock:

Modelling and data comparison

Jerker Jarsjö and Georgia Destouni

Water Resources Engineering
Royal Institute of Technology, Stockholm

November 1998

Keywords: Degassing, Two-phase flow, Gas content, Gs saturation, Bubble trapping, Transmissivity, Phase occupancy, Fractured rock, Fracture aperture, Hydrologic testing

ABSTRACT

Dissolved gas may be released from deep groundwater in the vicinity of open boreholes and drifts, where the water pressures are relatively low. Degassing of groundwater may influence observations of hydraulic conditions made in drifts, interpretation of experiments performed close to drifts, and buffer mass and backfill performance, particularly during emplacement and repository closure. Under certain conditions, considerable fracture inflow and transmissivity reductions have been observed during degassing experiments in the field and in the laboratory; such reductions affect the outcome and interpretation of both hydraulic and tracer tests. We develop models for the estimation of the resulting degree of fracture gas saturation and the associated transmissivity reduction due to groundwater degassing in fractured rock. Derived expressions for bubble trapping probability show that fracture aperture variability and correlation length influence the conditions for capillary bubble trapping and gas accumulation. The laboratory observations of bubble trapping in an Äspö fracture replica are consistent with the prediction of a relatively high probability of bubble trapping in this fracture. The prediction was based on the measured aperture distribution of the Äspö fracture and the applied hydraulic gradient. Results also show that the conceptualisation of gas and water occupancy in a fracture greatly influences model predictions of gas saturation and relative transmissivity. Images from laboratory degassing experiments indicate that tight apertures are completely filled with water, whereas both gas and water exist in wider apertures under degassing conditions; implementation of this relation in our model resulted in the best agreement between predictions and laboratory observations. Model predictions for conditions similar to those prevailing in field for single fractures at great depths indicate that degassing effects in boreholes should generally be small, unless the gas contents are elevated above the range of natural gas contents at Äspö HRL; these results are consistent with field observations in boreholes. However, for a system of interconnected fractures, it is plausible that degassing could cause considerable transmissivity reductions in some of the fractures, which have high bubble trapping probabilities, while high relative transmissivities in the other fractures prevent local water pressure build-up and gas re-dissolution.

TABLE OF CONTENTS

1 INTRODUCTION

Methodologies for quantification of flow and transport properties of fractured rock have received much interest since the 1980's due to the planned final storage of radioactive waste in the bedrock in several countries. The concept for the storage of high-level radioactive waste preferred by the Swedish Nuclear Waste Management Company (SKB) involves the construction of a final repository in granite bedrock at 400-500 metres depth. Even though the design of the engineered barriers for waste containment is considered to be the most critical safety aspect for the disposal, the impact of the eventual failure of these barriers on the biosphere must also be considered. Hence one of the main goals for the research and development work at Äspö Hard Rock Laboratory (HRL) (see Bäckblom, 1991, for a detailed description) concerns the quality and appropriateness of different methods for characterising the bedrock, the link between the engineered barriers and the biosphere. For the failure scenario, the transport and conductive properties of rock is of particular interest.

Borehole pump tests and pressure recovery tests are standard techniques for the determination of the hydraulic properties of fractured rock. In the pump tests, water is either withdrawn at a constant rate while monitoring the borehole pressure, or the pressure is kept at a constant rate while monitoring the flow required to maintain the constant pressure. In the subsequent pressure recovery test, the borehole is closed and the increasing pressure is monitored as a function of time. The transient data are then typically evaluated through curve matching with analytical solutions (derived by Theis, 1935, for withdrawal tests and Horner, 1951, for recovery tests), whereby the transmissivity, storativity and flow geometry in the vicinity of the borehole may be estimated (see e.g. Almén et al., 1986, and Mishra, 1992, for extensive reviews of single-well hydraulic test methods). In addition to the hydraulic characterisation carried out in boreholes, drift inflow measurements are important for the hydraulic characterisation of larger rock masses. Water is then collected in ditches that cross the drift floor, and the total inflow versus time is measured for specific drift sections.

Groundwater degassing may contribute to the development of an unsaturated zone in fractures intersecting drifts or boreholes, which may affect the magnitude and distribution of inflow and the outcome of hydraulic tests. Groundwater degassing is, for instance, hypothesised to have contributed to such inflow reductions during a field experiment in the Stripa mine (Olsson, 1992; Birgersson et al., 1993; Long et al., 1995). If degassing of groundwater is a significant factor in controlling the hydrology near drifts, it is essential to know this when experiments are planned, executed and evaluated. A transient change in hydraulic properties due to two-phase flow conditions around drifts and deposition holes may affect conditions during emplacement of the engineered barriers. A reduction in hydraulic conductivity due to two-phase flow conditions may simplify emplacement of buffer material in deposition holes but may also delay saturation and swelling of the buffer mass.

The gas content in the water at 300-450 metres depth below the groundwater table at the Äspö HRL range between 0.1% and 3.3% (Geller and Jarsjö, 1995; Nilsson, 1997). Nitrogen is the major component, occupying approximately 80% of the total gas volume. The opening of boreholes and drifts at these depths imply considerable water pressure lowering and release of dissolved gas.

A series of laboratory and field investigations at the Äspö HRL was initiated with the objective to show if degassing of groundwater affect measurements of hydraulic properties in fractures intersecting boreholes and drifts. An additional objective, in case degassing effects could be observed, was to show under what conditions two-phase (or unsaturated) flow will occur and be significant (e.g., investigate the effect of dissolved gas contents, fracture aperture distribution, transmissivity and flow geometry). The main goal of the sub-programme carried out by the KTH Water Resources Engineering (WRE) group, herewith reported, was to develop quantitative models for the prediction of degassing effects, using laboratory and field test data as a basis. The laboratory and field testing have also been an important part of the KTH/WRE programme, and the results from these tests, which partly have been carried out in collaboration with the group of Jane Long at Lawrence Berkeley National Laboratory (California), are summarised in this report.

Three different borehole degassing tests at natural gas contents have been conducted in the field up to this date (Geller and Jarsjö, 1995; Jarsjö and Destouni, 1997; Jarsjö and Destouni, 1998). In these tests, the fracture transmissivity was measured before and after allowing degassing to occur, and for all cases, there was no measurable transmissivity reduction that could be attributed to groundwater degassing.

However, in laboratory measurements, using transparent replicas of rock fractures originating from the Äspö HRL and the Stripa mine, gas phase development and significant transmissivity reduction were observed for dissolved gas contents exceeding a few percent (Jarsjö and Geller, 1996). To test these findings in the field, the natural gas contents at Äspö HRL were elevated through a dipole test, where gas saturated water was injected in one borehole and a degassing test was performed in a nearby (withdrawal) borehole. In this case, the fracture transmissivity was reduced to about half of the original transmissivity for an evolved gas content of 15% (Jarsjö and Destouni, 1997; Jarsjö and Destouni, 1998). Model results that were consistent with such a field observation indicated that similarly favourable conditions for the occurrence of degassing effects may occur around drifts at natural gas contents as around boreholes at an elevated gas content of 15% (Jarsjö and Destouni, 1998).

In this study, we develop models for estimation of the steady-state degree of fracture gas saturation and transmissivity reduction due to groundwater degassing in fractured rock. The model predictions are compared with observations of groundwater degassing in the laboratory and the field.

A mechanism that influences the degree of gas saturation in the fracture is the capillary trapping of evolved gas bubbles. Hunt et al. (1988) studied the capillary trapping mechanism for non-aqueous bubbles in porous media, and showed that trapping can lead to high non-aqueous phase saturations, because the ganglia and lenses cannot be mobilised by groundwater extraction under the conditions typically encountered in porous aquifers. However, the pore geometry of a fracture or a fracture system differs considerably from a porous medium geometry, and one may hypothesise that the probability for bubble trapping could be considerably lower in fractured media as compared with porous media, both because of high water velocities in wide fractures and small capillary pressure differences in

smooth fractures. Herein, we develop a tool for comparative analysis of the bubble trapping probability in fractures with different aperture distributions, subjected to various boundary conditions.

Furthermore, we develop relations between the dissolved gas content of the water, the steady-state degree of fracture gas saturation and the associated relative transmissivity (i.e., the ratio between unsaturated transmissivity and saturated transmissivity), using a statistical description of the fracture aperture. The quantities used in the statistical description of aperture distribution can be measured directly from rock samples (see Hakami, 1995), which implies that fewer fitting parameters are required as compared to corresponding relations commonly used for quantification of unsaturated porous medium flow (e.g., Brooks and Corey, 1964; Mualem, 1976; van Genuchten, 1980).

The above-mentioned porous medium relations for unsaturated flow are based on the assumption that the non-aqueous phase occupies the smaller pores and the aqueous (wetting) phase occupies the larger pores. A phase occupancy relation for fractured media, similar to porous medium assumption, was formulated by Pruess and Tsang (1990), who defined a critical cut-off aperture, above which gas exists as a separate phase and below which water exists as a separate phase. However, it has been recognised that the preferential occupation of wider apertures by the gas phase may in some cases be considerably violated due to phase accessibility. For instance, a wide aperture region may be surrounded by a tighter region and hence be inaccessible to the gas phase (Pyrak-Nolte et al., 1992; Murphy and Thomson, 1993). For degassing, it is also plausible that the preferential gas occupation of wide apertures can be violated for other reasons; for instance, because evolved bubbles may be swept away by the water flow in smoother fractures, i.e., in fractures where viscous drag dominates over capillary forces. In this study, we formulate two alternative phase occupancy relations that may be relevant for degassing in fractured rock, and investigate their influence on model predictions and agreement with experimental observations.

2 OBSERVATIONS

2.1 LABORATORY OBSERVATIONS

2.1.1 Degassing experiments

Degassing experiments in transparent epoxy replicas of rock fractures from the Stripa mine and the Äspö HRL were conducted in the laboratory with converging, radial flow (Jarsjö and Geller, 1996). The fractures of Jarsjö and Geller (1996) were completely water saturated before gas saturated water was introduced into the fracture. At first, the water pressures were kept above the bubble pressure which prevented a separate gas phase to develop. Then, the outlet pressures were lowered below the bubble pressure and gas started to develop in the fracture. The steady-state gas saturation and relative transmissivity were measured for each experiment.

Table 2-1. Degassing laboratory experiments conducted by Jarsjö and Geller (1996).

Experiment	Bubble pressure (kPa)	Gas (CO_2) content (%)
Stripa-1%	1.34	1.3
Stripa-3%	3.79	3.5
Äspö-3%a	3.45	3.2
Äspö-3%b	3.79	3.5
Äspö-7%a	7.58	7.0
Äspö-15%a	16.5	15.2

A total of seven experiments were conducted in replicas of one Stripa fracture and one Äspö fracture (Jarsjö and Geller, 1996). In the seventh and last experiment, the Äspö fracture replica was considerably deformed, implying that the results from this experiment is not comparable with the other Äspö fracture replica results. Therefore, this experiment will be excluded in the following description. Table 2-1 summarises the bubble pressure (in kPa above the (atmospheric) outlet pressure) and the evolved gas content (volume CO_2 per volume water) of the other six experiments.

2.1.2 Fracture aperture distribution

Our interpretation of the laboratory and field results is based on a statistical description of the fracture aperture. The aperture distribution of the laboratory fractures had prior to the degassing experiments been determined by saturating the replicas with dyed water and measuring the light transmission through the fracture; the relation between light transmission and the fracture aperture was determined using apertures with known width (Jarsjö and Geller, 1996). In Figure 2-1, we compare the measured aperture distribution of the Äspö fracture with the log-normal probability density function (pdf):

$$f_{\ln}(x;\mu_x,\sigma_x) = \frac{1}{x\sigma_x\sqrt{2\pi}}\exp\left(-\frac{1}{2\sigma_x^2}(\ln x-\mu_x)^2\right) \qquad (1)$$

where x is the log-normally distributed random variable, μ_x is the mean value of ln x and σ_x is the standard deviation of ln x. We matched a log-normal pdf for the aperture a ($f_{\ln}(a;\mu_a,\sigma_a)$; $f_{\ln}$ being defined through (1)) with the experimental data by choosing the (μ_a, σ_a)-pair that maximised the residual sum of squares (R^2) value. Figure 2-1 shows the best match (R^2=0.96), which was obtained for μ_a=-2.44 (geometric mean aperture a^G=exp[μ_a]=0.087 mm) and σ_a=0.88.

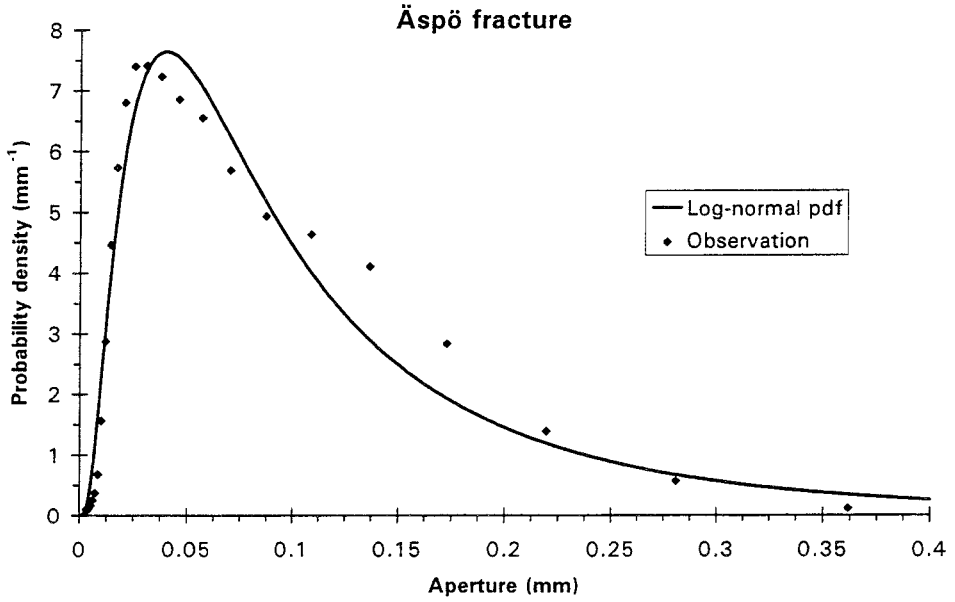

Figure 2-1 *Observed aperture distribution of the Äspö fracture compared with the best fitted log-normal pdf.*

The match between the Stripa aperture distribution and pdf (1) was poor. Therefore, we fitted a bimodal log-normal pdf:

$$f_{2\ln}(x;\mu_1,\sigma_1,\mu_2,\sigma_2,\upsilon) = \frac{\upsilon}{x\sigma_1\sqrt{2\pi}}\exp\left(-\frac{1}{2{\sigma_1}^2}\left(\ln x-\mu_1\right)^2\right) + \\ + \frac{1-\upsilon}{x\sigma_2\sqrt{2\pi}}\exp\left(-\frac{1}{2{\sigma_2}^2}\left(\ln x-\mu_2\right)^2\right) \quad (2)$$

which is a combination of two log-normal distributions, where distribution 1 is described by $f_{\ln}(x;\ \mu_1,\ \sigma_1)$ and distribution 2 is described by $f_{\ln}(x;\ \mu_2,\ \sigma_2)$. The coefficient υ of Equation (2) satisfies $0<\upsilon<1$ and represents the weight of distribution 1; the weight of distribution 2 is hence $(1-\upsilon)$. Figure 2-2 shows the best match between the experimental aperture data and $f_{\ln}(a;\ \mu_1,\ \sigma_1,\ \mu_2,\ \sigma_2,\ 0.3)$. The R^2-value was 0.97, and μ_1 and σ_1 for log-normal distribution 1 were -1.85 and 0.460, respectively. For log-normal distribution 2, μ_2 and σ_2 were -1.35 and 0.195, respectively.

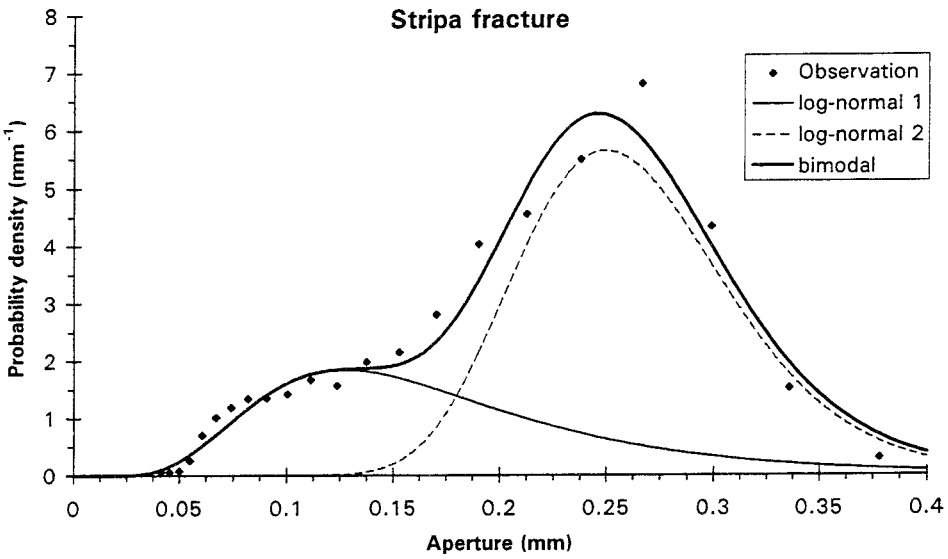

Figure 2-2 *Observed aperture distribution of the Stripa fracture compared with the best fitted bimodal pdf.*

2.1.3 Hydraulic and mechanical aperture

Before conducting the degassing experiments, the saturated transmissivity T of the Äspö and the Stripa fracture was estimated from the observed

flowrates. Based on these transmissivity values, we may estimate an equivalent hydraulic aperture (a_h) through the cubic law:

$$a_h = \sqrt[3]{\frac{12\mu_l T}{\rho g_0}} \tag{3}$$

where μ_l is the liquid viscosity, ρ is the liquid density and g_0 is the gravitational constant. The cubic law is valid for laminar flow between parallel plates where the aperture is constant. Hence, the hydraulic aperture for a rough (rock) fracture with transmissivity T is actually a measure of an equivalent separation distance required between two parallel plates to obtain the same transmissivity T as for the rough fracture.

In Table 2-2, the hydraulic apertures of the Äspö and Stripa fractures are compared with the corresponding measured mean apertures (or mechanical apertures) $\bar{a}$, obtained by arithmetic averaging of the measured, local fracture aperture values (see also Jarsjö and Geller, 1996). Previous investigations have indicated ratios $\bar{a}/a_h$ that range from 1.1 to 1.7 (Hakami, 1995). Table 2-2 shows that $\bar{a}/a_h$ for the Äspö fracture was 2.4 and for the Stripa fracture 2.1, both values being slightly above the range of Hakami (1995).

Table 2-2. Hydraulic aperture a_h and (mechanical) mean aperture $\bar{a}$ for the Äspö and the Stripa fracture (from Jarsjö and Geller, 1996).

Fracture	a_h (mm)	$\bar{a}$ (mm)
Äspö	0.045	0.11
Stripa	0.11	0.23

In this study, we will in the following estimate fracture transmissivities through application of the cubic law on local aperture values obtained from light intensity measurements (see the previous section). Since the presence of tight aperture regions may lower the effective fracture transmissivity to a relatively large extent, the cubic law approximation generally implies that the modelled effective transmissivity will be higher than the corresponding observed one (see, e.g., Persoff and Pruess, 1995). However, the use of the cubic law approximation can often be justified on the basis that it provides a reasonable approximation for the system under study (Murphy and Thomson, 1993). In the following, we use the cubic law approximation for

modelling the relative fracture transmissivity (defined as the ratio of unsaturated and the saturated transmissivity), and we compare different relative transmissivity models with experimental data. Through this comparison, we at least obtain some indication of model accuracy.

2.2 FIELD OBSERVATIONS

Four field degassing tests have been conducted at the Äspö HRL. The pilot hole test was conducted in borehole KA2512A at approximately 300 metres depth below the water table (Geller and Jarsjö, 1995), the three other tests were conducted in the boreholes KXTP2, KXTP4 and KXTP8 (abbreviated P2, P4 and P8, respectively) at approximately 450 metres depth below the water table (Jarsjö and Destouni, 1997; Jarsjö and Destouni, 1998).

Table 2-3. Field degassing tests (as summarised in Jarsjö and Destouni (1998)) characterised by their: borehole pressures at no flow (p_{nf}), borehole pressures during the degassing test (p_{bh}), estimated steady-state evolved gas content during the test ($\Delta\theta_g$) and corresponding bubble pressures (p_b), and observed (effective) relative transmissivity $T_{rel,obs}$, i.e., the ratio of the transmissivity before the degassing test and during/ after the degassing test.

Test hole	Test type[a]	p_{nf} (kPa)	p_{bh} (kPa)	$\Delta\theta_g$ (%vol)	p_b (kPa)	$T_{rel,obs}$ (m)
P2	SW	2000	36	2.4	160	0.89
P4	SW	1000	115	0.1	121	0.93
P4-P8	DP	1000	107	15	957	0.53
KA2512	SW	3000	120	1	167	0.90

[a] SW = single-well test; DP = dipole test

Table 2-3 summarises the conditions prevailing during the degassing tests (see Jarsjö and Destouni, 1998 for further details). Three of the tests were performed as single-well tests, whereas the test performed in boreholes P4-P8 was a dipole test, where gas saturated water was injected in borehole P4 at the same time as the degassing test was performed in the (withdrawal) borehole P8. Significant flow reduction (corresponding to a relative transmissivity of 0.53) was observed only in the dipole test at the relatively high evolved gas content of 15% (Table 2-3). Due to measurement uncertainties and changes in boundary conditions during the testing, the

observed relative transmissivity values of about 0.9 in the three other tests can not be attributed to degassing (Geller and Jarsjö, 1995; Jarsjö and Destouni 1997; Jarsjö and Destouni, 1998).

3 THEORY DEVELOPMENT

3.1 BUBBLE TRAPPING PROBABILITY

The physical characteristics of the fracture aperture, such as the aperture variability and the correlation length, influence the steady-state gas saturation. For instance, in a smooth aperture with constant width, there are no capillary pressure differences over the evolved bubbles and hence the bubbles would be advected by the water, yielding an average steady-state gas saturation of the fracture that equals the evolved gas content. In contrast, for a rough fracture, the capillary pressure differences over a bubble would typically be great, leading to high bubble trapping probabilities and accumulation of gas in the fracture. Then, the steady-state gas content would be much greater than the dissolved gas content.

In order to relate the physical fracture aperture characteristics to a bubble trapping probability, we use the equilibrium relation that the difference in capillary pressure upstream and downstream of a trapped bubble (Δp_c) equals the corresponding difference in water pressure (Δp_w; caused by the hydraulic gradient over the fracture).

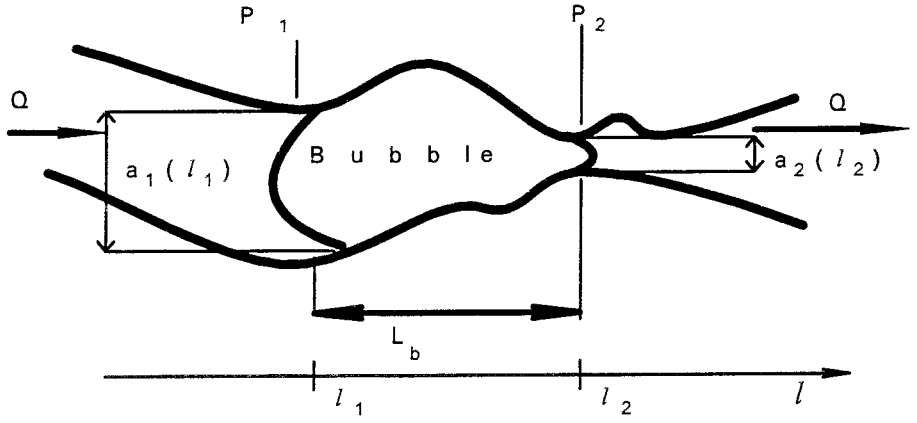

Figure 3-1 *Trapped gas bubble in a variable aperture fracture.*

Using the notation of Figure 3-1, and assuming that the pressure gradient is (dp/dl) along the mean flow direction, the difference in water pressure over the bubble becomes $\Delta p_w = p_1 - p_2 = L_b(dp/dl)$, where L_b is the bubble length

along the mean flow direction l. Furthermore, the difference in capillary pressure over the bubble is $\Delta p_c=2\sigma_w(1/a_2-1/a_1)$, where σ_w is the surface tension of water and a_1 and a_2 are the apertures upstream and downstream the bubble, respectively. Using the above-mentioned equality between Δp_c and Δp_w that is required for bubble trapping, the length L_b of a trapped bubble may be expressed as a function of the apertures a_1 and a_2:

$$L_b = 2\sigma_w\left(\frac{dp}{dl}\right)^{-1}\left(\frac{1}{a_2}-\frac{1}{a_1}\right) \tag{4}$$

In the following, we consider a variable aperture fracture for which the aperture a_i at location $l=l_i$ along the mean flow direction can be described statistically with a log-normal pdf (Equation (1)), characterised by the mean value μ_a and standard deviation σ_a. The probability for a bubble of length L_b, extending from $l=l_1$ to $l=l_2$, to be trapped is the probability that equality (4) is true. In (4), the apertures a_1 at l_1 and a_2 at l_2 are random variables, and it is therefore uncertain whether or not an aperture combination $a_1(l_1)$ and $a_2(l_2)$ can be found such that the distance $l_2-l_1=L_b$, as it must be for the equality (4) to be true. The probability for such an aperture combination to occur can be quantified from a derived probability density function (pdf) for L_b on basis of the pdf's for a_1 and a_2.

To derive a pdf for L_b, we first assume that the correlation length λ of the variable aperture fracture is much smaller than L_b, such that there is no correlation between the aperture values $a_1(l_1)$ and $a_2(l_2)$. For log-normal a, the pdf for the quantity $b_2=1/a_2$ is also log-normal with a mean value of $\mu_{b2}=-\mu_a$ and a standard deviation of $\sigma_{b2}=\sigma_a$ and is hence given by:

$$f_{b2}(b_2) = f_{\ln}(b_2;-\mu_a,\sigma_a) \quad \text{for} \quad 0 < b_2 \leq \infty \tag{5}$$

where the log-normal pdf $f_{\ln}$ is defined through Equation (1). Furthermore, the pdf for the quantity $b_1=(-1/a_1)$ is given by:

$$f_{b1}(b_1) = f_{\ln}(-b_1;-\mu_a,\sigma_a) \quad \text{for} \quad -\infty \leq b_1 < 0 \tag{6}$$

The resulting pdf for the difference $z=(-1/a_1)+1/a_2=b_1+b_2$ is then given by convolution of $f_{b1}(b_1)$ and $f_{b2}(b_2)$:

$$f(z) = \int_{-\infty}^{0} f_{b1}(b_1) \cdot f_{b2}(z - b_1) db_1 \qquad (7)$$

We can now obtain the pdf for $L_b = 2\sigma_w \cdot (dp/dl)^{-1} \cdot z$ (see Equation (4)) by use of the fact that $f(z)dz = f(L_b)dL_b$ and hence $f(L_b) = |dz/dL_b| f(z)$, or:

$$f(L_b) = \frac{(dp/dl)}{2\sigma_w} \int_{-\infty}^{0} f_{b1}(b_1) \cdot f_{b2}\left(\frac{L_b (dp/dl)}{2\sigma_w} - b_1 \right) db_1 \qquad (8)$$

The pdf $f(L_b)$ can be used to quantify the probability for a bubble of the specific length L_b to occur in the fracture due to capillary trapping under the given gradient (dp/dl). The pdf given by Equation (8), however, is mathematically defined throughout the range $(-\infty \leq L_b \leq \infty)$ and some of these mathematically possible L_b-values, such as for instance negative values, are physically not meaningful as lengths of trapped bubbles. By formulating relevant physical constraints for the bubble lengths that can possibly be trapped in a given fracture, we may estimate the probability for this range of possible bubbles to occur as the area below the pdf $f(L_b)$ between the limits given by the maximum and minimum possible L_b-values.

Figure 3-2(a) shows a schematic graph of a derived pdf $f(L_b)$ for uncorrelated a_1 and a_2. One constraint for the physically possible lengths of trapped bubbles (Figure 3-1) is that the length L_b must be greater than the local aperture value. Spherical bubbles, for instance, would otherwise be too small to connect both opposite fracture surfaces. Assuming that the fluctuations of a are small (small perturbation assumption) one may formulate this constraint as $L_b \geq \overline{a}$ (with the minimum bubble length then becoming $L_{b,min} = \overline{a}$), where $\overline{a}$ is the mean aperture. At this stage, the pdf $f(L_b)$ and the above expression for $L_{b,min}$ is not only valid for degassing applications, but is generally relevant for gas bubble trapping between two rough surfaces. For degassing applications, we can add the constraint that $L_b \leq X_{low}$ (with the maximum bubble length then becoming $L_{b,max} = X_{low}$), where X_{low} is the extent of the low-pressure zone (read: the extent of the zone where pressures are lower than the bubble pressure under water saturated conditions and where degassing can possibly occur).

The shaded area between the vertical lines in Figure 3-2(a) thus represents the probability for bubbles with lengths between $L_{b,min}$ and $L_{b,max}$ to be

trapped in a fracture with a small correlation length (uncorrelated aperture case). The effect of an increased pressure gradient (dp/dl) on the bubble trapping probability is illustrated in Figure 3-2(b), where $f(L_b)$ was calculated for the same fracture as shown in Figure 3-2(a), but with (dp/dl) being twice as high as that in Figure 3-2(a). For this higher gradient, the relevant probability area below $f(L_b)$ is smaller (Figure 3-2(b)), which implies that bubble trapping is less likely to occur. Hence, the probability for bubble trapping decreases with increasing pressure gradients.

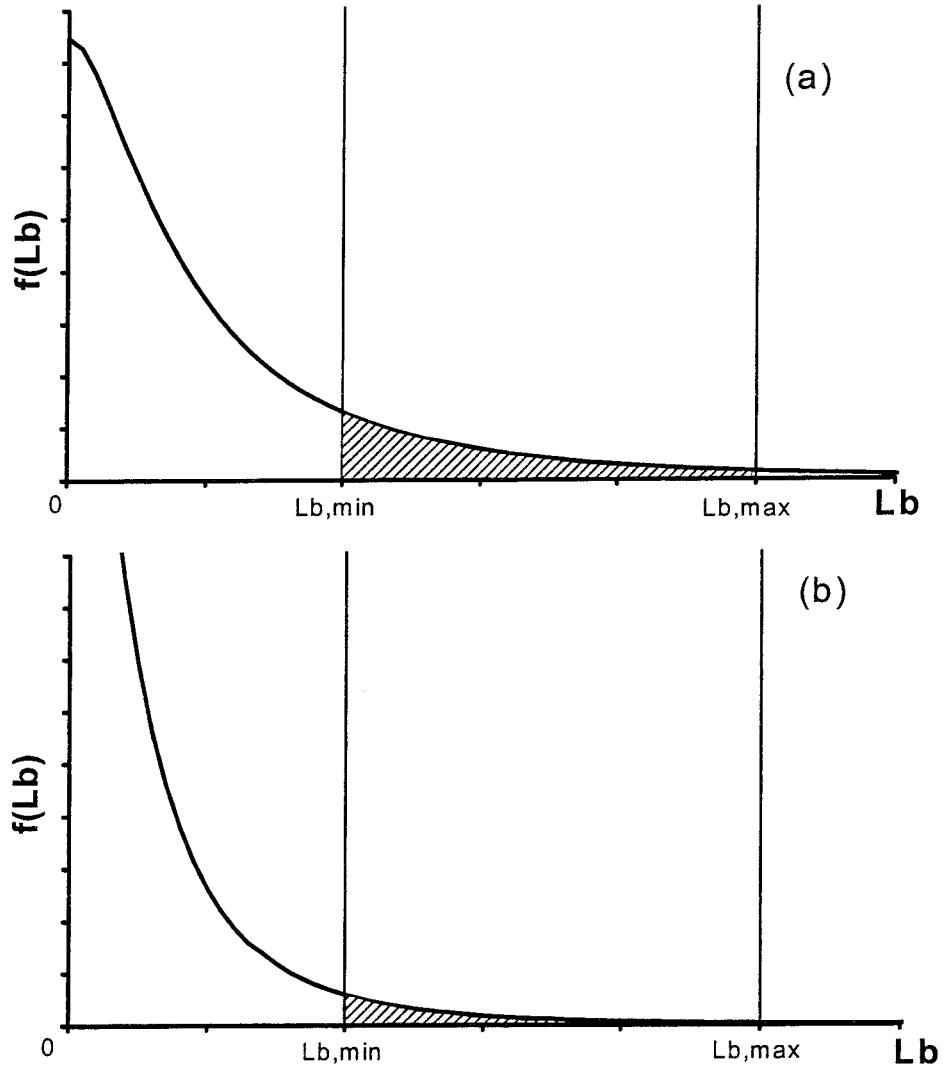

Figure 3-2 *(a) Schematic graph of the derived pdf $f(L_b)$, and (b) the pdf $f(L_b)$ for the same fracture as in (a) but with the pressure gradient being twice the gradient of (a). The axes in (a) and (b) are shown in the same scale.*

Equation (8) was derived under the assumption that the correlation length λ of the variable aperture fracture is much smaller than L_b. We now consider

larger λ-values, such that there is a correlation between the aperture values $a_1(l_1)$ and $a_2(l_2)$. Using the same notation as for Equations (7)-(8) the pdf for z in the correlated case becomes:

$$f(z;h) = \frac{d}{dz} \int_{-\infty}^{0} \int_{0}^{z-b_1} f_j(-b_1, b_2; -\mu_a, \sigma_a, h) db_1 db_2 \tag{9}$$

and since $f(z)dz=f(L_b)dL_b$ the pdf for L_b becomes:

$$f(L_b;h) = \frac{d}{dL_b} \int_{-\infty}^{0} \int_{0}^{L_b \cdot A - b_1} f_j(-b_1, b_2; -\mu_a, \sigma_a, h) db_1 db_2 \tag{10}$$

where $A=(dp/dl)/(2\sigma_w)$ and f_j is a joint two-variable log-normal pdf that is consistent with the marginal one-variable log-normal pdf (1), and is given by:

$$f_j(x_1, x_2; \mu, \sigma, h) = \frac{1}{2\pi x_1 x_2 \sqrt{\sigma^4 - C^2}} \cdot \exp\left(- \frac{\sigma^2 (\ln x_1 - \mu)^2 - 2C(\ln x_1 - \mu)(\ln x_2 - \mu) + \sigma^2 (\ln x_2 - \mu)^2}{2(\sigma^4 - C^2)} \right) \tag{11}$$

where x_1 and x_2 are the spatially correlated, random, variables at positions l_1 and l_2, respectively, being separated by a distance $h=l_2-l_1$ (along the mean flow direction; Figure 3-1). In (11), $C = \sigma^2 \cdot \exp(-\lambda / h)$ is an assumed exponential and isotropic auto-correlation function for the random variable x, which is assumed stationary, having the same mean value μ and the same standard deviation σ at all locations, l.

In contrast to the previously discussed uncorrelated case, the actual form of $f(L_b;h)$ (Equation (10)) for correlated apertures $a_1(l_1)$ and $a_2(l_2)$ (relatively large correlation length λ) depends on the separation distance $h=l_2-l_1$ through the joint pdf f_j (11). The bubble trapping equality (4), on which Equation (10) is based, is physically meaningful only for a bubble length L_b that equals the actual separation distance $h=l_2-l_1$ between the apertures $a_1(l_1)$ and $a_2(l_2)$ (see Figure 3-1). This implies that each pdf $f(L_b;h)$ (10) yields only one probability density value relevant for bubble trapping, namely the value for

$L_b=h, f(L_b=h;h)$. Figure 3-3 shows pdf's $f(L_b;h)$ (10) for different values of h. Each pdf is in Figure 3-3 associated with a vertical line, which illustrates the bubble trapping probability density value for $L_b=h$. Hence for correlated fracture apertures, bubble trapping probability densities for different bubble lengths L_b stem from different pdf's (as shown by the vertical lines in Figure 3-3). This is in contrast to the uncorrelated case, where the bubble trapping probability densities for different L_b-values were all given by the same pdf (8). This difference implies that a bubble trapping probability relevant for a range of bubble lengths (between the limits $L_{b,min}$ and $L_{b,max}$) can not be defined in the same way in the correlated case as in the uncorrelated case, where a single pdf (given by (8)) was integrated over the considered range of L_b-values. However, for a given bubble length L_b, the bubble trapping probability densities given by (8) and (10) may be used for comparative purposes, in order to determine whether bubble trapping is more probable in the uncorrelated or the correlated case.

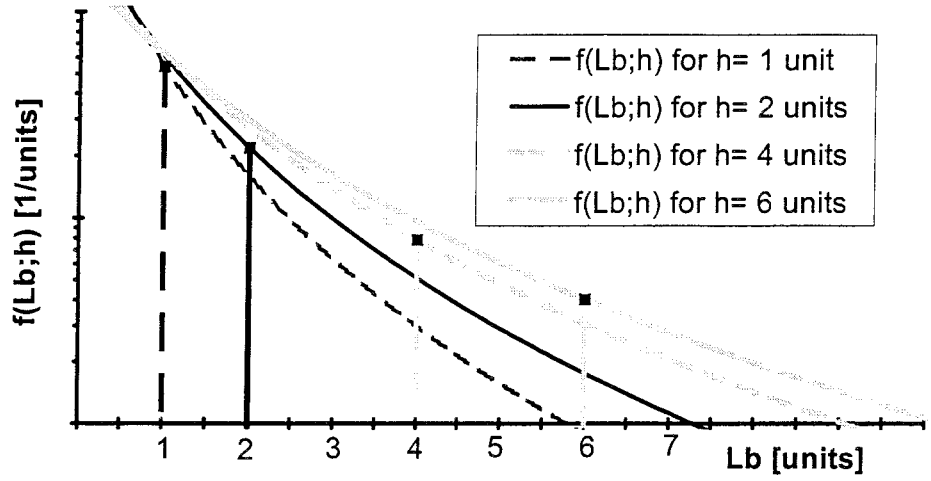

Figure 3-3 *Pdf's $f(L_b;h)$ for correlated apertures $a_1(l_1)$ and $a_2(l_2)$ with different values of the separation distance h. The vertical lines represent bubble trapping probability density values $f(L_b=h;h)$. The y-axis is in logarithmic scale.*

3.2 BUBBLE PRESSURE - SATURATION - RELATIVE TRANSMISSIVITY RELATIONS

In this study, we use a direct statistical description of the fracture aperture as a basis for the relations describing fracture saturation and relative transmissivity. The advantage of using aperture statistics based relations

rather than the porous medium type of relations for unsaturated flow (e.g., Brooks and Corey, 1964; Mualem, 1976; van Genuchten, 1980) is that fewer fitting parameters are required once the distribution of the aperture has been measured. In contrast to soils samples, where the pore size distribution is measured indirectly, there are methods for direct measurement of the aperture distribution of rock fracture samples (see, e.g., Hakami, 1995).

Furthermore, the statistical description enables us to directly investigate the effect of underlying critical hypotheses relevant for a gas phase evolved due to degassing in fractured rock. More specifically, one critical hypothesis regards the gas and water phase occupancy in different regions of the variable aperture fracture at steady-state. Figure 3-4(b) shows an image of the gas occupancy in different fracture regions of the Äspö laboratory fracture under degassing conditions (Jarsjö and Geller (1996)); Figure 3-4(a) shows the same fracture under water saturated conditions, before the degassing experiment. The fracture plane is parallel to the plane of the paper and the dark regions represent wide apertures; the fracture aperture decreases with decreasing darkness. The white regions of the fracture in Figure 3-4(b) are occupied by gas. Figure 3-4 suggests that gas occupies the wider apertures and water the tighter; however, it seems that water also exists in certain parts of the wide aperture regions. In order to evaluate the possible effects of water occupying also some parts in wide aperture regions, we will in the following formulate two different phase occupancy relations and evaluate the influence of each relation on the model predictions.

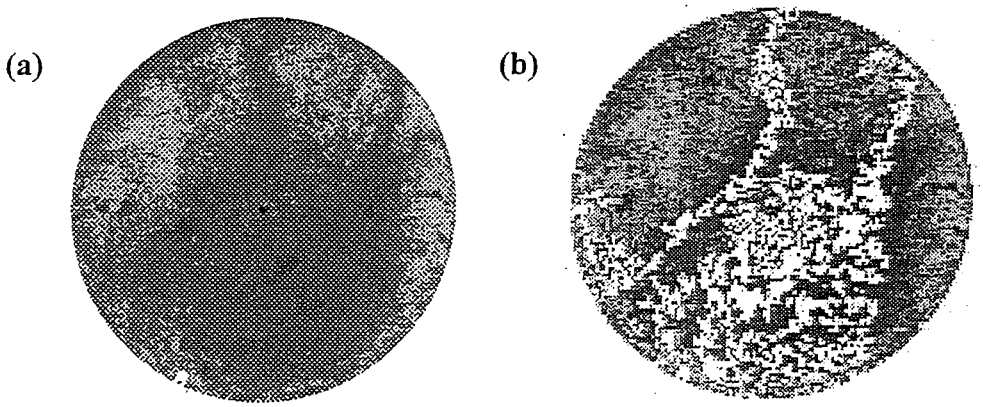

Figure 3-4 *(**a**) The water saturated Äspö laboratory fracture, and (**b**) the gas phase occupancy in the Äspö fracture at steady-state degassing conditions.*

3.2.1 Relations for different phase occupancy assumptions

In the first phase occupancy relation, we assume that there is a critical aperture, below which water (only) exists as a separate phase and above which gas (only) exists as a separated phase. A similar assumption underlies, e.g., the Brooks-Corey and van Genuchten relations for porous media, namely that pores exceeding a certain width are filled with gas whereas pores that are smaller than this width are water filled. We refer to this relation as the separation assumption ($phase_S$):

$$phase_S = \begin{cases} w \text{ if } a < a_c \\ g \text{ if } a \geq a_c \end{cases} \tag{12}$$

where a_c is the critical cut-off aperture, w denotes water occupancy and g denotes gas occupancy. An underlying assumption for (12) is that the bubble trapping probability is high, so that evolved gas bubbles actually are immobilised and accumulated throughout the wide aperture region, where $a \geq a_c$.

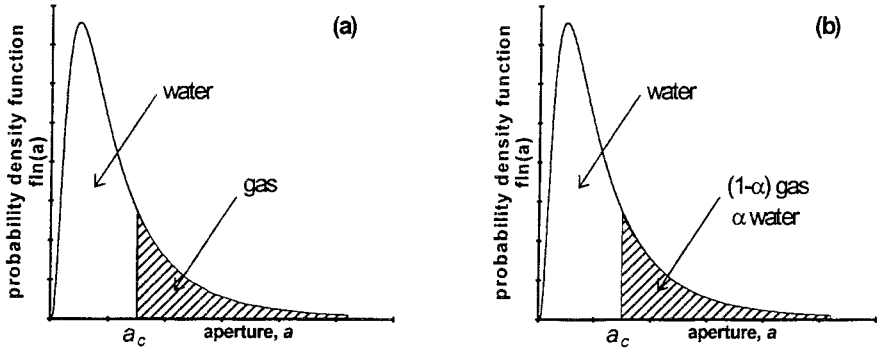

Figure 3-5 *Water and gas occupancy in a fracture with log-normal aperture distribution, using* ***(a)*** *the separation assumption* $phase_S$ *(12) and* ***(b)*** *the mix assumption* $phase_M$ *(13).*

We refer to the second phase occupancy relation, which is consistent with the gas occupancy observation in the Äspö fracture (Figure 3-4), as the mix assumption ($phase_M$):

$$phase_M = \begin{cases} w \text{ if } a < a_c \\ \alpha \cdot w + (1-\alpha) \cdot g \text{ if } a \geq a_c \end{cases} \tag{13}$$

where $0<\alpha<1$. In other words, in (12) we assume that the wide aperture region (where $a \geq a_c$) is completely filled with gas, whereas we in (13) assume that both gas and water may exist in the wide aperture region, by allowing a certain fraction α of the region to be occupied by water (illustrated in Figure 3-5). The actual value of α is related to the degree of bubble trapping in the fracture aperture. For instance, assuming that the fracture is smooth, so that capillary trapping effects are negligible, the degree of gas saturation in the fracture under degassing conditions equals the evolved gas content that then provides an upper constraint for α. For increasing degrees of bubble trapping, the degree of fracture gas saturation in the wide aperture regions approaches unity, due to accumulation of gas bubbles, which implies that α approaches 0.

Based on the pdf for a ($f_{\ln}(a)$), and a relevant expression for the phase occupancy, we may calculate the degree of fracture gas saturation as the volume of fracture filled with gas (V_{gas}) divided by the total fracture volume (V_{total}). The gas saturation S_S using the separation assumption (12) hence becomes:

$$S_S(a_c) = V_{gas}/V_{total} = \int_{a_c}^{\infty} a f_{\ln}(a)da \Big/ \int_{0}^{\infty} a f_{\ln}(a)da \qquad (14)$$

and for the mix assumption, the corresponding gas saturation S_M is:

$$S_M(a_c) = (1-\alpha)S_S(a_c) \qquad (15)$$

Furthermore, assuming that the cubic law holds locally, i.e., that the local transmissivity is proportional to the fracture aperture raised to the third power, we obtain the following expressions for the relative water transmissivities:

$$T_S(a_c) = T_{water}/T_{total} = \int_{0}^{a_c} a^3 f_{\ln}(a)da \Big/ \int_{0}^{\infty} a^3 f_{\ln}(a)da \qquad (16)$$

$$T_M(a_c) = T_S(a_c) + \alpha \int_{a_c}^{\infty} a^3 f_{\ln}(a)da \Big/ \int_{0}^{\infty} a^3 f_{\ln}(a)da \qquad (17)$$

where T_S is the relative transmissivity using the separation assumption (12) and T_M is the relative transmissivity using the mix assumption (13).

In order to obtain a relation between the gas content of the water and the steady-state degree of gas saturation in the fracture, we first need to relate the dissolved gas concentration C_g and the cut-off aperture a_c. In the following, we will use the bubble pressure p_b as a measure of C_g. Under equilibrium conditions, the bubble pressure is related to C_g through Henry's law:

$$p_b = HC_g \tag{18}$$

where p_b is the bubble pressure in kPa (abs), H is Henry's law constant for the gas in the liquid in kPa·m^3·mol^{-1}, and C_g is the molar concentration of gas dissolved in the liquid. Assuming that equilibrium prevails, gas will not exist as a separate phase in the fracture if the local aperture is such that the corresponding gas phase pressure p_g would exceed the bubble pressure p_b. From the relation between the capillary pressure difference p_c (being defined as the difference between the water pressure, p_w, and the gas pressure, p_g) and the fracture aperture a, we obtain

$$p_c = p_g - p_w = \frac{2\sigma_w}{a} \tag{19}$$

where σ_w is the water surface tension. From (19), we may then express the critical cut-off aperture a_c, below which p_g would exceed p_b, by substituting p_b for p_g and a_c for a in (19), yielding:

$$a_c = \frac{2\sigma_w}{p_b - p_w} \tag{20}$$

3.2.2 Effective parameters for radial flow configuration

We now consider radial, converging, steady-state flow in a horizontal fracture. The fracture inlet pressure equals p_{in} along the outer radius $r=R$. The fracture outlet pressure along the well radius $r=r_w$ ($r_w<R$) equals p_{out} ($<p_{in}$). Due to the spatial variations in local water pressures p_w that occur under flow, the cut-off aperture a_c (20) will be a function of both the bubble pressure p_b and the radial coordinate r (through the dependence of p_w on r).

The dependence between a_c and r implies that there is also a variation in gas saturation S and relative transmissivity T_{rel} within the fracture plane. With the aim to estimate effective parameters relevant for the fracture as a whole, we discretise the fracture into n circular segments of radial thickness $\Delta r = (R - r_w)/n$. The radial coordinate of the mid-point of segment j is then given by $r_j = r_w + (R - r_w)(j + 0.5)/n$. For steady-state, radial flow in a horizontal fracture, Darcy's law in combination with the equation of continuity yield the following relation between the pressure drop over a segment and the transmissivity of the segment:

$$\Delta p_1 = C_0 \frac{\Delta r}{T_1 r_1} = \Delta p_2 = C_0 \frac{\Delta r}{T_2 r_2} = \ldots = \Delta p_n = C_0 \frac{\Delta r}{T_n r_n} \tag{21}$$

where C_0 is a constant. From the boundary condition that the total pressure drop over the fracture equals the difference between inlet and outlet pressures

$$\Delta p_{tot} = \sum_{i=1}^{n} \Delta p_i = C_0 \sum_{i=1}^{n} \frac{\Delta r}{T_i r_i} = (p_{in} - p_{out}) \tag{22}$$

we can determine the constant C_0 in relation (21), which gives the following expression for the pressure difference over segment j with transmissivity T_j:

$$\Delta p_j = \frac{p_{in} - p_{out}}{\sum_{i=1}^{n} \frac{\Delta r}{T_i r_i}} \cdot \frac{\Delta r}{T_j r_j} \tag{23}$$

We assume that water saturated conditions prevail from the start, implying that the local, relative transmissivities T_j equal unity. The water pressure in each segment j is obtained from:

$$p_{w,j} = p_{out} + \sum_{n=1}^{j} \Delta p_j \tag{24}$$

where Δp_j is given by (23). The cut-off aperture for segment j is:

$$a_{c,j} = \frac{2\sigma_w}{p_b - p_{w,j}} \tag{25}$$

New values for the local relative transmissivities, $T_{j,new}$ are then obtained from Equations (16) or (17) with $a_c=a_{c,j}$. The next relative transmissivity estimate ($T_{j,N+1}$; the estimate of iteration number (N+1)) is chosen between the previous estimate $T_{j,N}$ and the new estimate $T_{j,new}$ according to:

$$T_{j,N+1} = \beta T_{j,new} + (1-\beta) T_{j,N} \tag{26}$$

where $0<\beta<1$. In order to avoid oscillations in the numerical iteration, the factor β is kept sufficiently low for the transmissivity estimates to monotonically approach the final value.

New values of the resulting segment pressures for iteration N+1, $\Delta p_{j,N+1}$, are obtained by substituting $T_{j,N+1}$ for T_j in Equation (23). When $\Delta p_{j,N+1} \approx \Delta p_{j,N}$ and $T_{j,N+1} \approx T_{j,N}$, the local saturation S_j in segment j, with cut-off pressure $a_{c,j}$, is obtained from Equations (14) or (15), depending on phase occupancy assumption. The effective relative transmissivity $T_{rel,eff}$, relevant for the fracture as a whole, is then obtained from the averaging of the local segment relative transmissivities T_j:

$$T_{rel,eff} = \frac{1}{n}\sum_{j=1}^{n} T_j \tag{27}$$

Since the area of the segments increase with increasing values of r, the total degree of fracture gas saturation is obtained by weighting each segment saturation by the corresponding segment area:

$$S_{tot} = \frac{1}{R^2 - r_w^2}\sum_{j=1}^{n} S_j\left(\left(r_j + \Delta r/2\right)^2 - \left(r_j - \Delta r/2\right)^2\right) \tag{28}$$

4 RESULTS AND IMPLICATIONS

4.1 BUBBLE TRAPPING ESTIMATION AND OBSERVATIONS

The trapped bubble length pdf $f(L_b)$ assuming uncorrelated fracture apertures $a_1(l_1)$ and $a_2(l_2)$ (Figure 3-1 and Equation (8)) was calculated using the fracture aperture statistics and maximum hydraulic gradient for the Äspö fracture replica (used in the laboratory degassing experiments of Jarsjö and Geller, 1996). This pdf is plotted as a grey curve in Figure 4-1. In addition, the vertical lines shown in Figure 4-1 represent probability densities $f(L_b=h;$ $h)$ for bubble trapping in the Äspö fracture assuming correlated $a_1(l_1)$ and $a_2(l_2)$ (Equation (10), Figure 3-3), with aperture correlation lengths λ of (a) 0.01 m and (b) 0.1 m. The figure shows that longer bubbles are less likely for the correlated cases than for the uncorrelated case. For instance, the probability density for a bubble length of 1 mm in the Äspö fracture is 173 m^{-1} for an uncorrelated aperture distribution, whereas the corresponding probability density is 78 m^{-1} for a correlation length of 1 cm and 12 m^{-1} for a correlation length of 1 dm. Hence, in addition to increasing gradients, increasing values of λ decrease the probability for longer bubbles. The reason is that the difference between apertures $a_1(l_1)$ and $a_2(l_2)$ (Figure 3-1) on average is smaller if these apertures are correlated than if they are uncorrelated. Smaller difference between $a_1(l_1)$ and $a_2(l_2)$, in turn, implies smaller capillary pressure differences over the bubble, which requires L_b to be shorter for bubble trapping to occur, i.e., for equilibrium to prevail between the capillary forces and the water pressure difference over the bubble length (see Equation (4)).

As shown in the theory development section, an estimate of the bubble trapping probability for uncorrelated fracture apertures may be obtained as the area below the pdf $f(L_b)$ between the minimum and maximum limits for physically possible L_b-values ($L_{b,min}$ and $L_{b,max}$). Taking the $L_{b,min}$-value as the mean aperture value ($\bar{a}$) of $1.1 \cdot 10^{-4}$ metres for the Äspö fracture (indicated by the vertical line to the left of the shaded area in Figure 4-2), and the $L_{b,max}$-value as the low-pressure zone extent of 0.058 metres for the Äspö fracture (outside the range of the graph of Figure 4-2), the bubble trapping

probability for the Äspö fracture is indicated by the shaded area of Figure 4-2. The figure shows that the relevant area below $f(L_b)$ (i.e., the area between the physical limits) constitutes a large fraction of the total area below $f(L_b)$ for positive L_b, which implies that the bubble trapping probability should be high in this fracture, assuming uncorrelated apertures. Furthermore, Figure 4-1 for correlated fracture apertures suggests smaller probabilities for long bubbles, however the probabilities for smaller bubble lengths (that still are above the $\bar{a}$-value of $1.1 \cdot 10^{-4}$ metres) are large in all cases. Such relatively high predicted bubble trapping probabilities are consistent with the experimental observations of an immobile gas phase development in the Äspö fracture by Jarsjö and Geller (1996).

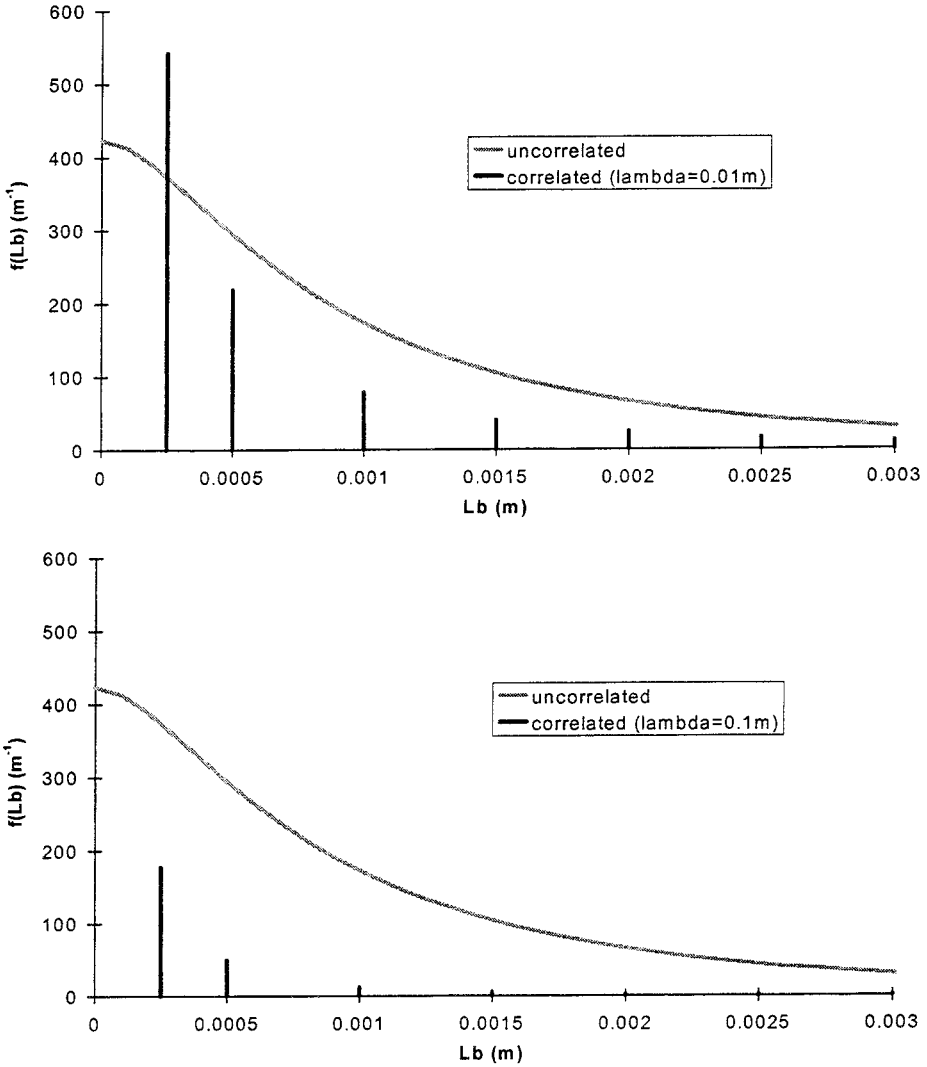

Figure 4-1 *Comparison of bubble trapping probabilities between an uncorrelated fracture aperture distribution (grey curve) and correlated distributions (black bars) with* ***(a)*** λ*=0.01 m and* ***(b)*** λ*=0.1 m.*

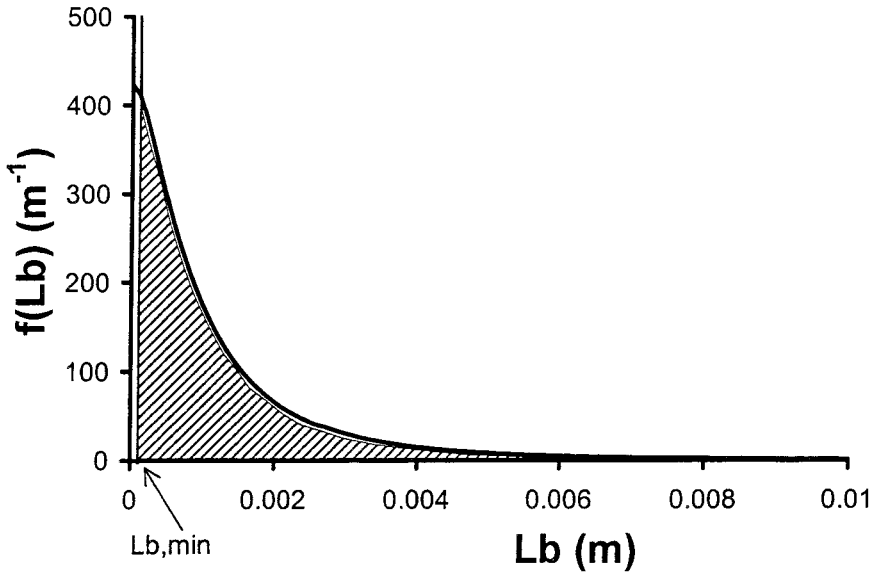

Figure 4-2 *The pdf $f(L_b)$ for the aperture distribution and maximum hydraulic gradient from the laboratory measurements in the Äspö fracture, assuming uncorrelated apertures a_1 and a_2.*

The presented methodology of calculating a probability for trapping of bubbles of different lengths between the limits $L_{b,min}$ and $L_{b,max}$ based on the derived pdf $f(L_b)$ provides a tool for comparative, rather than absolute, analysis of the possibility of immobile gas phase development due to degassing in different fractures. Furthermore, the bubble trapping probability may also provide information for phase occupancy relations and possibly the value of α in phase occupancy relation (13); however, for investigation of such possible relations there is a need for additional degassing observations in fractures of different aperture distribution.

4.2 SATURATION AND RELATIVE TRANSMISSIVITY

4.2.1 Influence of phase occupancy relation on the model results

Figure 4-3 illustrates the influence of assumed phase occupancy relation (the separation assumption (12) or the mix assumption (13) with water occupancy fraction α=0.2 in the wide aperture regions) on the pressure, saturation and relative transmissivity distribution in the Äspö fracture replica (μ_a=-2.44; σ_a=0.88; R=57.5mm; r_w=1.6mm) with a bubble pressure (p_b) of 8 kPa. The inlet pressure p_{in} at $r=R$ was set to p_b and the outlet pressure at $r=r_w$ was set to 0.

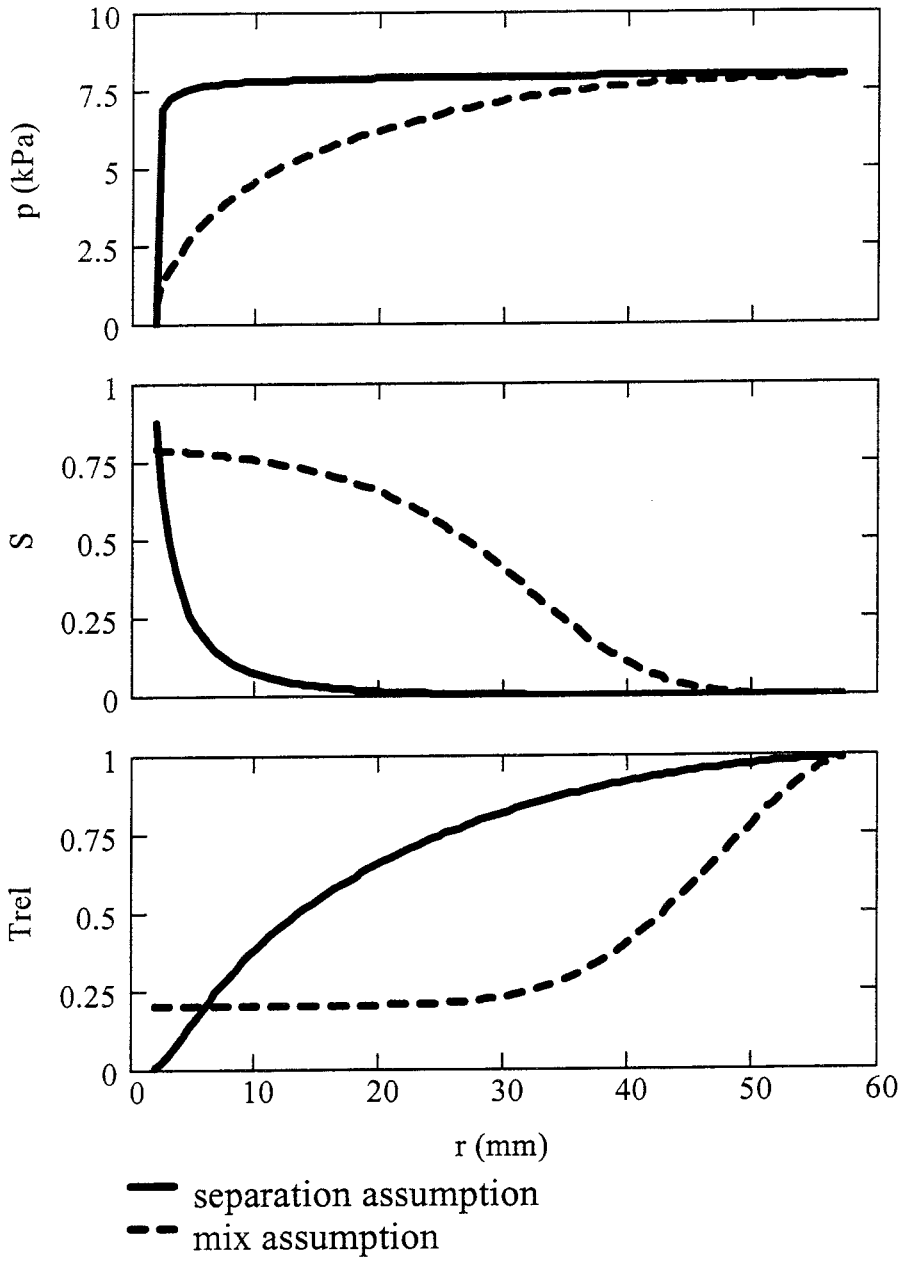

Figure 4-3 *Influence of phase occupancy relation on pressure, saturation and relative transmissivity.*

Figure 4-3 illustrates that the separation assumption (12; solid line) yields a higher saturation and a much lower relative transmissivity than the mix assumption (13; dashed line) at the fracture outlet (r=1.6), where the pressure is fixed to zero. In fact, for the same water pressure, the separation assumption generally yields a higher saturation and a lower transmissivity, as indicated by Equations (14)-(17). However, Figure 4-3 also shows that the water pressures p_w for the separation assumption (12) increase much more rapidly in the vicinity of the outlet due to the blocking effect caused by the considerably reduced transmissivities in the outlet region. Therefore, the

modelled water pressures are lower throughout the fracture using the mix assumption (13), resulting in a generally higher gas saturation and lower relative transmissivity than with the separation assumption (12). These differences are considerable, as shown in Figure 4-3.

4.2.2 Comparison with laboratory observations

We modelled the laboratory experiments of Jarsjö and Geller (1996) using the boundary condition that the fracture inlet pressure (p_{in} at $r=R$) is equal to the bubble pressure of the water in the saturation tank. At steady-state, this condition was approximately obtained in the laboratory for the Äspö-7%, the Äspö-3%b and the Stripa-3% experiments (see Table 2-1 for a list of the conducted experiments). For the Äspö-3%a, Äspö-15% and the Stripa-1% experiments, the final fracture inlet pressures at steady-state were 50% lower, or more, than the bubble pressure of the water in the saturation tank (Jarsjö and Geller, 1996). Under such conditions, the bubble pressure of the water entering the fracture is not known, because the water may have degassed to a certain degree already before entering the fracture. Depending on whether the water at the fracture inlet was supersaturated ($p_b>p_{in}$) or not ($p_b \leq p_{in}$), the actual condition in the laboratory for these three experiments may therefore have been more, equally or less favourable for a fracture gas phase evolution than the modelled condition.

Figure 4-4 shows the modelled degree of gas saturation S_{tot} as a function of the bubble pressure in the Äspö fracture using the separation assumption (solid line) and the mix assumption with $\alpha=0.05$ (dashed line), $\alpha=0.2$ (dotted line) and $\alpha=0.4$ (circles). The gas saturation degree observed in the four laboratory experiments with the Äspö fracture (Jarsjö and Geller, 1996) is in Figure 4-4 indicated with a thin solid line and crosses. The bubble pressure is expressed in kPa above the outlet pressure (that equalled the atmospheric pressure). Figure 4-4 shows that the separation assumption underestimates the degree of gas saturation by approximately an order of magnitude, whereas the agreement between prediction and observations is good using the mix assumption with α-values between 0.2 and 0.4. Generally, the predicted steady-state gas saturation increases with α for lower α-values (for the case shown in Figure 4-4, the saturation is higher for $\alpha=0.2$ and $\alpha=0.4$ than for $\alpha=0.05$). The reason for this increase is that increasing α implies lower pressures throughout the fracture, due to a diminishing blocking effect at the outlet (see section 4.2.1). However, the

total estimated degree of gas saturation based on the mix assumption cannot exceed (1-α) (see S_M in Equation 15), implying that increases in α have small effects on S_{tot} for intermediate values of α; this is also illustrated by the relatively small difference between the curves for α=0.2 and α=0.4 in Figure 4-4. For α-values that are sufficiently high for the blocking effect at the outlet to no longer dominate, S_{tot} decreases with increasing α, and approaches zero as α approaches unity.

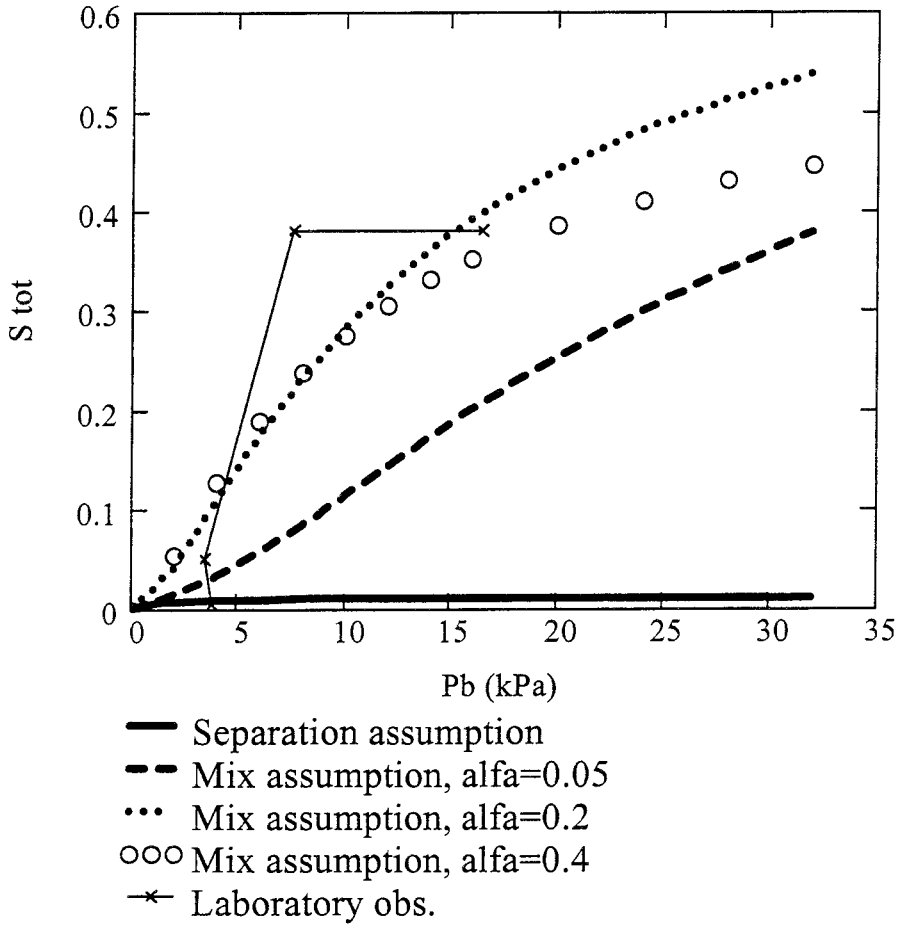

Figure 4-4 *Predicted and observed gas saturation degree in the Äspö fracture.*

Figure 4-5 shows the effective relative transmissivities $T_{rel,eff}$ for the same cases as shown in Figure 4-4 for the gas saturation. Note that the two observations of $T_{rel,eff}$ at $p_b \approx 4$ kPa were biased by the presence of a separate gas phase in the fracture inlet tubing. Without the influence of this gas phase, the observed $T_{rel,eff}$ would have been higher (see Jarsjö and Geller, 1996). The best match between prediction and observation is obtained using the mix assumption with α=0.2, whereas the separation assumption yield the poorest predictions. Generally, the transmissivity predictions are higher than

observations. However, a comparison between Figure 4-4 and Figure 4-5 shows that the same model and α-value yield the best fit both with respect to the degree of gas saturation and the effective relative transmissivity.

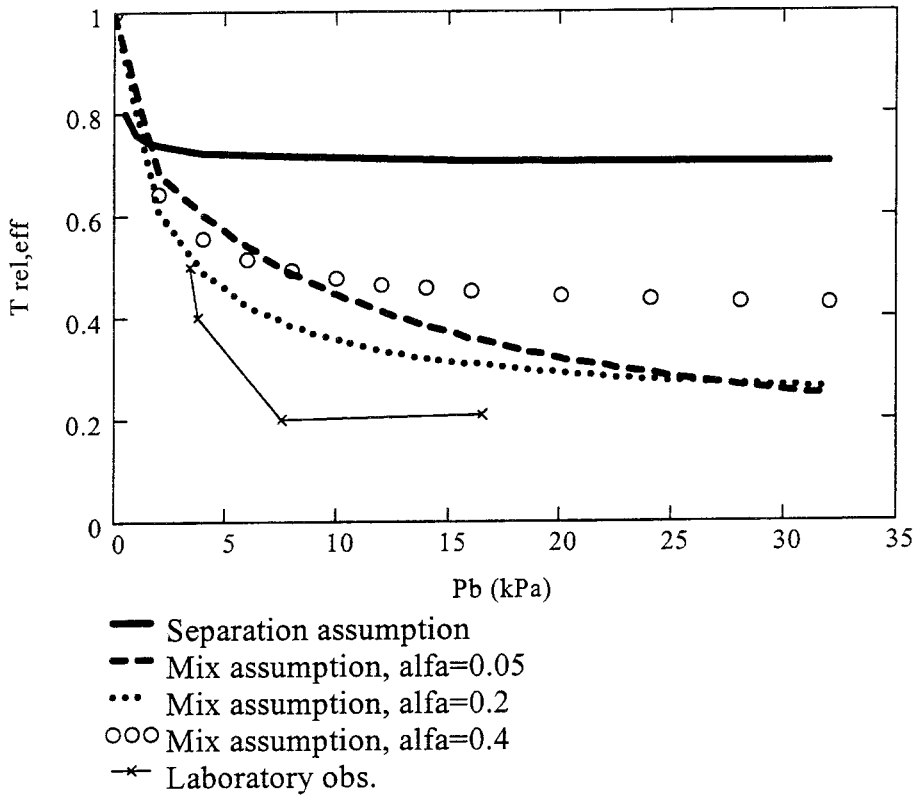

Figure 4-5 *Predicted and observed effective relative transmissivity in the Äspö fracture.*

In addition to the observations for the Äspö fracture, two experiments were conducted in the Stripa fracture at relatively low dissolved gas contents (1% and 3%, respectively). We modelled these experiments using the bimodal probability density function shown in Figure 2-2, hence substituting $f_{1\ln}(a)$ for $f_{2\ln}(a)$ in Equations (14), (16) and (17). The best fits between observations and predictions were in this case obtained using the mix assumption with α-values between 0.5 and 0.6. The model prediction of the Stripa 1% experiment then yielded a low value of the gas saturation and a high effective relative transmissivity (1.3% and 0.92, respectively), which is consistent with the observed gas saturation of 2% and a measured effective relative transmissivity equalling unity. For the Stripa 3% experiment, the difference between observed gas saturation and predicted gas saturation was larger (13% observed and 5% modelled) and so was the difference between observed and predicted effective relative transmissivity (0.58 observed and 0.83 modelled).

In summary, the mix assumption could provide acceptable fits to observations for both the Äspö fracture and the Stripa fracture, with water occupancy fractions, α, in the wide aperture regions ranging between 0.2 and 0.6, i.e., with 20% - 60% water occupying regions with apertures larger than the cut-off aperture a_c. The resulting match was generally good, however the observed effective relative transmissivities were slightly lower than the predicted ones. The model results are sensitive to the choice of phase occupancy assumption, (12) or (13), and there was a great discrepancy between the model predictions based on the separation assumption (12) and the mix assumption (13).

4.2.3 Comparison with field observations

A gas content of 3%, which has been observed at the Äspö Hard Rock Laboratory at 300-450 metres depth (Geller and Jarsjö, 1995; Nilsson, 1997), corresponds to a nitrogen bubble pressure of 200 kPa. This bubble pressure is much lower than the expected hydrostatic water pressure of up to 4500 kPa that can be expected at these depths. This difference implies that the radial extent of the possible degassing zone, where water pressures are lower than the bubble pressures, is limited to the near-borehole region (see Jarsjö and Destouni, 1998).

Figure 4-6 shows an illustration example of the influence of the ratio between boundary (or fracture inlet) pressure and bubble pressure on the total gas saturation degree and (effective) relative transmissivity for radial flow. The fracture assumed in this example had a geometric mean aperture of $a^G = \exp[\mu_a] = 0.025$ mm, and a (ln a) standard deviation of σ_a=0.8. This mean aperture value yields (through the cubic law) a transmissivity that is within the observed transmissivity range for the fractures used in the degassing tests with gas saturated water (conducted at Äspö HRL; Jarsjö and Destouni, 1998), and the standard deviation is similar to the measured standard deviation of the Äspö fracture replicas in the laboratory experiments of Jarsjö and Geller (1996).

In Figure 4-6, the ratio between the well radius r_w and the fracture radius (commonly denoted radius of influence) R is assumed to be $5 \cdot 10^{-4}$, which for instance is relevant for a borehole with r_w=3 cm and R=60 m. The example shown in Figure 4-6 is relatively insensitive to the value of R and the results

for, e.g., a borehole with r_w=3 cm and R=200 metres are approximately the same. We have furthermore used the mix phase occupancy assumption (13) with α=0.2, which resulted in a reasonably good agreement between predictions and observations for the degassing laboratory experiments (Figures 4-4 and 4-5).

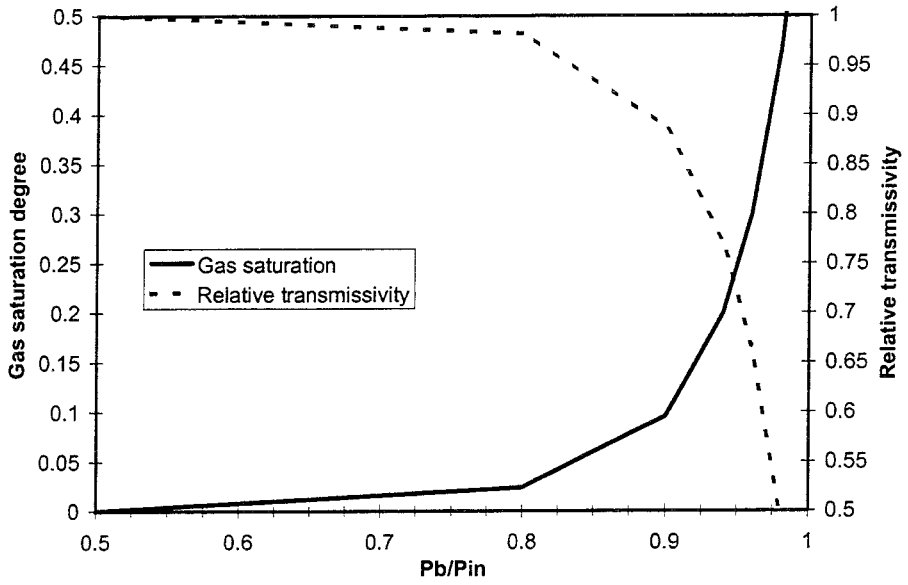

Figure 4-6 *Illustration example: Gas saturation degree and relative transmissivity as functions of the p_b/p_{in}-ratio.*

Figure 4-6 shows that the p_b/p_{in} ratio needs to be high (larger than 0.5) in order to get a considerable gas saturation in the fracture and a reduction in the (effective) relative fracture transmissivity. For comparison with borehole field test results from Äspö HRL, we use the p_b/p_{nf} ratio from the field (where p_{nf} is the borehole pressure at no flow conditions) as an analogue to the p_b/p_{in} ratio of Figure 4-6. Table 2-3 summarises the field degassing tests, showing that the p_b/p_{nf} ratio was low, ranging between 0.056 and 0.12, for all the single-well degassing tests conducted at Äspö. The fact that no considerable flow reduction was observed during these tests is consistent with the implications of Figure 4-6, i.e., that the gas saturation degree and the relative transmissivity reduction should be insignificant in boreholes with small p_b/p_{in} ratios.

In contrast, the p_b/p_{nf} ratio for the dipole degassing test was high (0.96). In this test, the observed relative transmissivity was reduced to 0.53 under degassing conditions. The p_{nf} value for this dipole test is not analogue to the radial flow p_{in} of Figure 4-6, both because of the influence of the nearby

drift on p_{nf} and because of the dipole flow geometry. However, we may note that for a similar p_b/p_{in} ratio Figure 4-6 implies a considerable degassing effect with a relative transmissivity of about 0.5, which is consistent with the value 0.53 in the dipole field experiment.

5 CONCLUSIONS

In this study, we have developed a model for estimation of the steady-state degree of fracture gas saturation and the potential transmissivity reduction due to groundwater degassing in fractured rock. We have also shown that the model predictions compare favourably with observations of groundwater degassing effects (or lack of effects) in both the laboratory and the field.

Because the gas contents in field are generally low (5% or less; Geller and Jarsjö, 1995; Nilsson, 1997), we do not expect high local degrees of gas saturations or measurable transmissivity reductions in the field, unless the evolved bubbles are trapped and accumulated in the fracture. In order to compare the possible degree of gas accumulation due to capillary trapping in different fractures under various conditions, we use a statistical aperture description and consider the probability density for differences in capillary pressures over a given fracture length. By also considering pressure gradients and physical restrictions on bubbles trapped by capillary forces, we obtained expressions for bubble trapping probability for both uncorrelated and correlated aperture values. These expressions are not only valid for degassing applications, but are generally relevant for gas bubble trapping between rough surfaces.

The bubble trapping probability increases with increasing aperture variability, and decreases with increasing water pressure gradients. In addition, the trapping probability decreases with increasing aperture correlation length, particularly for larger bubble lengths. The derived expressions indicated that the bubble trapping probability of the Äspö fracture used in the laboratory experiments of Jarsjö and Geller (1996) was relatively high, which is in agreement with the observation of a considerable gas phase development in this fracture.

Derived relations between the water gas content (or bubble pressure), and the resulting degree of gas saturation and relative transmissivity are also based on a statistical description of the fracture aperture. As compared with models commonly used for saturation and relative conductivity relations in porous media (e.g., Brooks and Corey, 1964; Mualem, 1976; van

Genuchten, 1980), the direct statistical description of fracture apertures requires fewer fitting parameters once the fracture aperture distribution is measured. In addition, the statistical description enables us to directly investigate the effect of underlying critical hypotheses relevant for a gas phase evolved due to degassing in fractured rock.

One such critical hypothesis that we have investigated here regards the gas and water phase occupancy in different regions of a variable aperture fracture at steady-state. Two alternative hypotheses were formulated, which we refer to as the separation assumption and the mix assumption. In the separation assumption, gas is assigned to all regions of the fracture where the local aperture value a is greater than or equal to a critical aperture a_c, and water is assigned to all regions were the local aperture is less than this critical aperture. In the mix assumption both gas and water are allowed in the wider aperture regions where $a \geq a_c$, whereas water only is allowed in the regions where $a < a_c$.

The developed model relates the gas content (or bubble pressure) to the critical aperture, which in turn is an explicit part of the expressions for gas saturation and relative transmissivity. Using a radial flow configuration to simulate degassing in the vicinity of an open borehole, we found that the model predictions were very sensitive to the choice of phase occupancy assumption. The separation assumption resulted in much lower predicted gas saturation and higher effective relative transmissivity (i.e., the ratio between unsaturated transmissivity under degassing conditions and saturated transmissivity) than the mix assumption. The reason is that the modelled water pressures generally were much higher using the separation assumption, due to a blocking effect caused by considerably reduced transmissivities in the near-borehole region; higher water pressures imply that gas to a greater extent remains solved in the water phase.

Comparison between model predictions and laboratory observations (Jarsjö and Geller, 1996) showed poor agreement in terms of both gas saturation and relative transmissivity when using the separation assumption for different bubble pressures. The corresponding agreement using the mix assumption was good for a water occupancy that ranged between 20% and 60% in the wide aperture regions ($a \geq a_c$). In addition, images of gas and water phase occupancy in the transparent Äspö fracture replica under

degassing conditions show that water does indeed exist to a certain extent in the wide-aperture regions, which is consistent with the mix phase occupancy assumption.

We also predicted the gas saturation and relative transmissivity for conditions similar to those prevailing during borehole tests in field, using the mix phase occupancy assumption that provided the best match with laboratory observations. We showed that the potential for considerable degassing effects depends on the ratio between the pressure at the boundary (or "inlet" pressure; p_{in}) and the bubble pressure (p_b); this ratio is generally low for the range of gas contents that have been measured in the field under natural conditions at 300-450 metres depth. For the three single-well borehole tests that were conducted in the field at natural gas contents at Äspö HRL (Geller and Jarsjö, 1995; Jarsjö and Destouni, 1997; Jarsjö and Destouni, 1998) the estimated p_b/p_{in} ratio was less than 0.12. No flow reduction due to degassing was observed during these single-well tests, which is consistent with modelled relative transmissivities close to unity for such a low p_b/p_{in} ratio. In contrast, a relative fracture transmissivity of 0.53 was observed under degassing conditions in the field during the dipole test (Jarsjö and Destouni, 1997; Jarsjö and Destouni, 1998), where gas saturated water was injected. The ratio between the no-flow borehole pressure and the bubble pressure was 0.96 for this test; the predicted relative transmissivity for a radial flow degassing experiment conducted with a correspondingly high p_b/p_{in}-ratio was also approximately 0.5.

Our investigation of the influence of the p_b/p_{in} ratio on predicted relative transmissivities for borehole test conditions indicated that the relative transmissivity will be close to unity for p_b/p_{in} less than 0.5. This implies that degassing effects in single fractures that intersect boreholes under field conditions would generally be small. Phenomena not considered in our model that could possibly enhance the effects of degassing somewhat are, for instance, violation of the local equilibrium assumption, caused by slow, rate-limited re-dissolution of evolved gas. However, for the case of borehole tests we do not expect such an effect to have a major influence on the relative fracture transmissivity, because the low-pressure zone where degassing possibly can occur is so small around boreholes (Jarsjö and Destouni, 1998).

The model results, however, showed that both boundary conditions (here expressed as the p_b/p_{in} ratio) and the physical characteristics of the fracture aperture may greatly influence the degree of gas saturation and transmissivity reduction due to degassing. Hence, in a system of interconnected fractures with different aperture characteristics, it is plausible that gas may accumulate in some of the fractures (having high bubble trapping probabilities) and cause considerable transmissivity reductions there. The transmissivities of the remaining connected fractures (with low bubble trapping probabilities) would in this case remain unaffected, and prevent a general pressure build-up and gas re-dissolution in the fracture zones where transmissivity reductions have occurred.

Interconnected fracture systems are mainly of interest for the case of groundwater degassing around drifts. A drift - borehole comparison (Jarsjö and Destouni, 1998) showed that degassing is more likely around drifts, because the extent of the low pressure zone is larger around drifts. The herewith reported results, in conjunction with the results of Jarsjö and Destouni (1998), imply that groundwater degassing is not likely to cause considerable inflow reductions around boreholes at natural gas contents, whereas degassing remains to be a plausible explanation for the observed inflow reductions to the drift in the Stripa mine (see Olsson, 1992; Birgersson et al., 1993; Long et al., 1995).

LIST OF SYMBOLS

a	-	Fracture aperture
a_1	-	Fracture aperture at location $l=l_1$ (upstream)
a_2	-	Fracture aperture at location $l=l_2$ (downstream)
a_c	-	Cut-off fracture aperture, above which gas may exist under equilibrium conditions
a^G	-	Geometric mean of fracture aperture
a_h	-	Hydraulic fracture aperture, defined through (3)
b_1	=	$-1/a_1$
b_2	=	$1/a_2$
C	-	An assumed exponential and isotropic auto-correlation function, equal to $\sigma^2 \cdot \exp(-\lambda / h)$ where σ denotes standard deviation
C_g	-	Molar concentration of gas dissolved in the liquid
f	-	Probability density function
f_{2ln}	-	One-variable, bimodal, log-normal probability density function
f_{b1}	-	Probability density function for the quantity b_1
f_{b2}	-	Probability density function for the quantity b_2
f_j	-	Joint two-variable, unimodal, log-normal probability density function
f_{ln}	-	One-variable, unimodal, log-normal probability density function
g	-	Gas phase occupancy
g_0	-	Gravitational constant
h	-	Separation distance along the mean flow direction, equal to l_2-l_1
H	-	Henry's constant in $kPa \cdot m^3 \cdot mol^{-1}$
l	-	Spatial coordinate along the mean flow direction
l_1	-	Coordinate for the upstream end of the bubble
l_2	-	Coordinate for the downstream end of the bubble
L_b	-	Length (along the mean flow direction) of a trapped bubble
$L_{b,max}$	-	Maximum limit for the length of a trapped bubble
$L_{b,min}$	-	Minimum limit for the length of a trapped bubble
n	-	Number of segments of the discretised fracture

N	-	Iteration counter
p_b	-	Bubble pressure, equal to HC_g under equilibrium conditions
p_{bh}	-	Borehole pressure
p_c	-	Capillary pressure, equal to p_g-p_w
p_g	-	Gas phase pressure
p_{in}	-	Fracture inlet pressure along the radius r=R
p_{nf}	-	Borehole pressure at no-flow conditions
p_{out}	-	Fracture outlet pressure along the radius r=r_w (p_{out}<p_{in})
p_w	-	Water phase pressure
r	-	Radial distance from the well centre ($r_w \leq r \leq R$)
r_w	-	Well radius
R	-	Radius of influence
S	-	Gas saturation degree, i.e., the fracture volume filled with gas divided by the fracture pore volume
S_M	-	Modelled S using the mix assumption (13)
S_S	-	Modelled S using the separation assumption (12)
S_{tot}	-	Total S, S_M or S_S, relevant for the fracture as a whole under radial flow conditions
T	-	Fracture transmissivity
T_M	-	Modelled T_{rel} using the mix assumption (13)
T_S	-	Modelled T_{rel} using the separation assumption (12)
T_{rel}	-	Relative transmissivity, i.e., the ratio between unsaturated transmissivity and saturated transmissivity
$T_{rel,eff}$	-	Effective T_{rel}, T_M or T_S, relevant for the fracture as a whole under radial flow conditions
w	-	Water phase occupancy
X_{low}	-	Low pressure zone extent, i.e., the extent of the zone where p_w<p_b under water saturated conditions
z	=	b_1+b_2
α	-	Assumed water occupancy fraction in fracture regions where a>a_c; corresponding gas occupancy is (1-α)
$\Delta\theta_g$	-	Evolved, volumetric gas content
λ	-	Aperture correlation length
μ_a	-	Mean value of ln a
μ_l	-	Liquid viscosity
ρ	-	Liquid density
σ_a	-	Standard deviation of ln a
σ_w	-	Surface tension of water

REFERENCES

Almén, K.-E., Andersson, J.-E., Carlsson. L., Hansson, K. and Larsson, N.-Å., 1986. Hydraulic testing in crystalline rock. A comparative study of single-hole test methods. SKB Technical Report 86-27.

Birgersson, L., Moreno, L., Neretniks, I., Widén, H. and Ågren, T., 1993. A tracer experiment in a small fracture zone in granite. Water Resour. Res., 29, 3867-3878.

Brooks, R. H. and Corey, A. T., 1964. Hydraulic properties of porous media. Hydrol. Pap. 3, Colorado State University, Fort Collins.

Bäckblom, G., 1991. The Äspö Hard Rock Laboratory - a step toward the Swedish final repository for high-level radioactive waste. Tunneling and underground space technology, 6, 463-467.

Geller, J. T. and Jarsjö, J., 1995. Groundwater degassing and two-phase flow: Pilot hole test report. SKB International Cooperation Report 95-03.

Hakami, E., 1995. Aperture distribution of rock fractures. PhD Thesis, Division of Engineering Geology, Royal institute of Technology, Stockholm.

Horner, D. R., 1951. Pressure build up in wells. Proc. Third World Pet. Cong., The Hague, Sect II, 503-523.

Hunt, J. R., Sitar, N. and Udell, K., 1988. Nonaqueous phase liquid transport and cleanup: 1. Analysis of mechanisms. Water Resour. Res., 24, 1247-1258.

Jarsjö, J. and Destouni, G., 1997. Groundwater degassing: Pilot injection - withdrawal field tests with gas saturated water. SKB Äspö HRL Progress Report HRL-97-02.

Jarsjö J. and Destouni, G., 1998. Degassing of groundwater in fractured rock around boreholes and drifts. Water Resour. Res. (in review).

Jarsjö, J. and Geller, J. T., 1996. Groundwater degassing: Laboratory experiments in rock fracture replicas with radial flow. SKB Äspö HRL Progress Report HRL-96-12.

Long, J. C. S., Olsson, O., Martel, S. and Black, J., 1995. Effects of excavation on water inflow to a drift. In: *Fractured and Jointed Rock Masses*, Proceedings of the conference on fractured and jointed rock masses, Lake Tahoe, California, edited by Myer, L.R., Tsang, C.-F., Cook, N.G.W. and Goodman, R.E., A.A. Balkema, Rotterdam, Brookfield, pp. 543-549.

Mishra, S., 1992. Methods for analyzing single- and multi-well hydraulic test data. In: *Interpretation of crosshole hydraulic tests and a pilot fluid logging test for selected boreholes within the BK-site*, edited by Vomvoris, S. and Frieg, B., NAGRA Technical Report 91-09, Wettingen.

Mualem, Y., 1976. A new model for predicting the hydraulic conductivity of unsaturated porous media. Water Resour. Res., 12, 513-522.

Murphy, J. R. and Thomson, N. R., 1993. Two-phase flow in a variable aperture fracture. Water Resour. Res., 29, 3453-3476.

Nilsson, A.-C., 1997. Water and gas analyses of groundwater sampled in the borehole KZ0027A. SKB Äspö HRL Progress Report HRL-97-15.

Olsson, O., 1992. Site characterization and validation - final report. SKB Stripa Project Technical Report 92-22.

Persoff, P. and Pruess, K., 1995. Two-phase flow visualization and relative permeability measurement in natural rough-walled fractures. Water Resour. Res., 31, 1175-1186.

Pruess, K. and Tsang, Y. W., 1990. On two-phase relative permeability and capillary pressure of rough-walled rock fractures. Water Resour. Res., 26, 1915-1926.

Pyrak-Nolte, L. J., Helgeson, D., Haley, G. M. and Morris, J. W., 1992. Immiscible fluid flow in a fracture. In: *Proceedings of the 33rd U.S. Rock Mechanics Symposium*, edited by Tillerson and Wawersik, A. A. Balkema, Rotterdam, Netherlands, pp. 571-578.

Theis, C.V., 1935. The relation between the lowering of the piezometric surface and the rate and duration of discharge of a well using ground-water storage. Am. Geophys. Union Trans., 16, 519-524.

van Genuchten, M. Th., 1980. A closed-form equation for predicting the hydraulic conductivity of unsaturated soils. Soil Sci. Soc. Am. J., 44, 892-898.

List of SKB reports

Annual Reports

1977-78
TR 121
KBS Technical Reports 1 – 120
Summaries
Stockholm, May 1979

1979
TR 79-28
The KBS Annual Report 1979
KBS Technical Reports 79-01 – 79-27
Summaries
Stockholm, March 1980

1980
TR 80-26
The KBS Annual Report 1980
KBS Technical Reports 80-01 – 80-25
Summaries
Stockholm, March 1981

1981
TR 81-17
The KBS Annual Report 1981
KBS Technical Reports 81-01 – 81-16
Summaries
Stockholm, April 1982

1982
TR 82-28
The KBS Annual Report 1982
KBS Technical Reports 82-01 – 82-27
Summaries
Stockholm, July 1983

1983
TR 83-77
The KBS Annual Report 1983
KBS Technical Reports 83-01 – 83-76
Summaries
Stockholm, June 1984

1984
TR 85-01
Annual Research and Development Report 1984
Including Summaries of Technical Reports Issued during 1984. (Technical Reports 84-01 – 84-19)
Stockholm, June 1985

1985
TR 85-20
Annual Research and Development Report 1985
Including Summaries of Technical Reports Issued during 1985. (Technical Reports 85-01 – 85-19)
Stockholm, May 1986

1986
TR 86-31
SKB Annual Report 1986
Including Summaries of Technical Reports Issued during 1986
Stockholm, May 1987

1987
TR 87-33
SKB Annual Report 1987
Including Summaries of Technical Reports Issued during 1987
Stockholm, May 1988

1988
TR 88-32
SKB Annual Report 1988
Including Summaries of Technical Reports Issued during 1988
Stockholm, May 1989

1989
TR 89-40
SKB Annual Report 1989
Including Summaries of Technical Reports Issued during 1989
Stockholm, May 1990

1990
TR 90-46
SKB Annual Report 1990
Including Summaries of Technical Reports Issued during 1990
Stockholm, May 1991

1991
TR 91-64
SKB Annual Report 1991
Including Summaries of Technical Reports Issued during 1991
Stockholm, April 1992

1992
TR 92-46
SKB Annual Report 1992
Including Summaries of Technical Reports Issued during 1992
Stockholm, May 1993

1993
TR 93-34
SKB Annual Report 1993
Including Summaries of Technical Reports Issued during 1993
Stockholm, May 1994

1994
TR 94-33
SKB Annual Report 1994
Including Summaries of Technical Reports Issued during 1994
Stockholm, May 1995

1995
TR 95-37
SKB Annual Report 1995
Including Summaries of Technical Reports Issued during 1995
Stockholm, May 1996

1996
TR 96-25
SKB Annual Report 1996
Including Summaries of Technical Reports Issued during 1996
Stockholm, May 1997

List of SKB Technical Reports 1998

TR 98-01
Global thermo-mechanical effects from a KBS-3 type repository. Summary report
Eva Hakami, Stig-Olof Olofsson, Hossein Hakami, Jan Israelsson
Itasca Geomekanik AB, Stockholm, Sweden
April 1998

TR 98-02
Parameters of importance to determine during geoscientific site investigation
Johan Andersson[1], Karl-Erik Almén[2], Lars O Ericsson[3], Anders Fredriksson[4], Fred Karlsson[3], Roy Stanfors[5], Anders Ström[3]
[1] QuantiSci AB
[2] KEA GEO-Konsult AB
[3] SKB
[4] ADG Grundteknik KB
[5] Roy Stanfors Consulting AB
June 1998

TR 98-03
Summary of hydrochemical conditions at Aberg, Beberg and Ceberg
Marcus Laaksoharju, Iona Gurban, Christina Skårman
Intera KB
May 1998

TR 98-04
Maqarin Natural Analogue Study: Phase III
J A T Smellie (ed.)
Conterra AB
September 1998

TR 98-05
The Very Deep Hole Concept – Geoscientific appraisal of conditions at great depth
C Juhlin[1], T Wallroth[2], J Smellie[3], T Eliasson[4], C Ljunggren[5], B Leijon[3], J Beswick[6]
[1] Christopher Juhlin Consulting
[2] Bergab Consulting Geologists
[3] Conterra AB
[4] Geological Survey of Sweden
[5] Vattenfall Hydropower AB
[6] EDECO Petroleum Services Ltd.
June 1998

TR 98-06
Indications of uranium transport around the reactor zone at Bagombe (Oklo)
I Gurban[1], M Laaksoharju[1], E Ledoux[2], B Made[2], A L Salignac[2],
[1] Intera KB, Stockholm, Sweden
[2] Ecole des Mines, Paris, France
August 1998

TR 98-07
PLAN 98 – Costs for management of the radioactive waste from nuclear power production
Swedish Nuclear Fuel and Waste Management Co
June 1998

TR 98-08
Design premises for canister for spent nuclear fuel
Lars Werme
Svensk Kärnbränslehantering AB
September 1998

TR 98-09
Test manufacturing of copper canisters with cast inserts
Assessment report
Claes-Göran Andersson
Svensk Kärnbränslehantering AB
Augusti 1998

TR 98-10
Characterization and Evaluation of Sites for Deep Geological Disposal of Radioactive Waste in Fractured Rocks
Proceedings from The 3rd Äspö International Seminar, Oskarshamn, June 10–12, 1998-11-10
Svensk Kärnbränslehantering AB
September 1998

TR 98-11
Leaching of 90-year old concrete mortar in contact with stagnant water
Jan Trägårdh, Björn Lagerblad
Swedish Cement and Concrete Research Institute
July 1998

TR 98-12
Geological structural models used in SR 97
Uncertainty analysis
Pauli Saksa, Jorma Nummela
FINTACT Ltd
October 1998

TR 98-13
Late Quaternary changes in climate
Karin Holmgren and Wibjörn Karlén
Department of Physical Geography
Stockholm University
December 1998

TR 98-14
Partitioning and transmutation (P&T) 1997
Åsa Enarsson, Anders Landgren, Jan-Olov Liljenzin, Mats Skålberg, Lena Spjuth
Department of Nuclear Chemistry, Chalmers University of Technology, Gothenburg
and
Waclaw Gudowski, Jan Wallenius
Department of Nuclear and Reactor Physics, Royal Institute of Technology, Stockholm
May 1998

TR 98-15
Studies of surface complexation of H^+, NpO_2^+, Co^{2+}, Th^{4+} onto TiO_2 and H^+, UO_2^{2+} onto alumina
Anna-Maria Jakobsson, Yngve Albinsson
Department of Nuclear Chemistry, Chalmers University of Technology, Sweden
and
Robert S Rundberg
Los Alamos National Laboratory, USA
November 1998

TR 98-16
Backfilling with mixtures of bentonite/ ballast mixtures or natural smectitic clay?
Roland Pusch
Geodevelopment AB
October 1998